Title	Influence of elastic anisotropy on the shapes of ellipsoidal blisters and stress field around the blisters in solid materials
Author(s)	Ishii, Akio
Citation	AIP Advances. 2023, 13(12), p. 125024
Version Type	VoR
URL	https://hdl.handle.net/11094/93376
rights	This article is licensed under a Creative Commons Attribution 4.0 International License.
Note	

Influence of elastic anisotropy on the shapes of ellipsoidal blisters and stress field around the blisters in solid materials
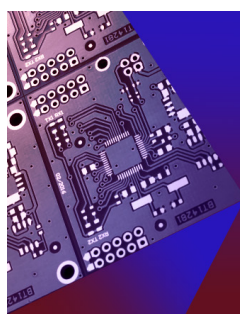
Akio Ishii ✉ 📧

Check for updates

View Online   Export Citation   CrossMark

Influence of elastic anisotropy on the shapes of ellipsoidal blisters and stress field around the blisters in solid materials

View Online   Export Citation   CrossMark

Akio Ishii[a] iD

AFFILIATIONS

Department of Mechanical Science and Bioengineering, Osaka University, Osaka 560-8531, Japan

[a]Author to whom correspondence should be addressed: ishii@me.es.osaka-u.ac.jp

ABSTRACT

To address the embrittlement challenges posed by gas blisters in anisotropic materials, the stable shape of constant-pressure blisters in anisotropic materials (hexagonal, tetragonal, and rhombohedral) was energetically investigated based on continuum theory (micromechanics), considering the blister as Eshelby's ellipsoidal inclusion. The non-negligible change in the blister shape was confirmed in terms of the anisotropic factor $\eta \equiv C_{3333}/C_{1111}$. Although the spherical shape of the blister is preferable for isotropic and cubic materials ($\eta = 1$), the x_3 normal penny and capsule shapes were theoretically confirmed to be the most stable ones for $\eta > 1$ and $\eta < 1$, respectively. The penny and capsule shape blisters generate larger stress fields around themselves than the sphere shape blisters, thus inducing crack formation. The embrittlement due to the gas (typically hydrogen or helium) inside the blister for the anisotropic materials was more significant than isotropic and cubic embrittlement.

I. INTRODUCTION

Gas bubbles, typically helium or hydrogen bubbles, are found in solid materials. The formation of such bubbles is being extensively investigated owing to the recent demand for hydrogen storage and nuclear materials in modern human society.[1–6] Bubbles form in such materials via the clustering of abundant vacancies, which are created by interactions of moving dislocations during deformation or irradiation, in addition to the rapid diffusion of the helium or hydrogen atom in the material. Clustered vacancies form a void and rapidly diffused atoms tend to accumulate in it, thereby forming bubbles.[7–14] Bubble formation in a material can significantly degrade its mechanical properties; essentially, these bubbles introduce local stress fields due to their internal pressure, thereby causing embrittlement of the material and facilitating blistering.[3,15–19]

The blisters, which are large-sized (ranging from hundreds of micrometers to a few millimeters) bubbles, are usually observed experimentally and are considered the starting points of cracks due to the stress field generated around them.[17,20,21] The stress fields formed around the blisters depend on their shape, i.e., penny,

capsule, or needle-like blisters generate larger stresses than spherical blisters around the sharp edge. Thus, to prevent embrittlement, the morphology of blisters formed in solid materials must be understood. The experimental observation of the detailed shape of the blisters is difficult, and theoretical investigations are necessary. In this study, we highlighted the relationship between the elastic anisotropy and the shape of the blisters formed in the solid material based on a conventional continuum theory, viz., micromechanics. Considering the blisters as an ellipsoidal secondary phase with a significantly small elastic constant $\tilde{C}_{ijkl} \approx 0$ in the matrix materials, we predicted the shape of the blister in terms of energy and investigated the stress field around it in the anisotropic materials using the famous Eshelby's ellipsoidal inclusion theory, which takes the anisotropy and the heterogeneity of elastic constants into consideration.[22–25]

II. METHODOLOGY

In this study, we consider the blister as an ellipsoid ($\frac{x_1^2}{a_1^2} + \frac{x_2^2}{a_2^2} + \frac{x_3^2}{a_3^2}$ = 1, where $\mathbf{x} = [x_1, x_2, x_3]$ indicates a position inside the matrix material and a_i is the half axis of the ellipsoid in each direction).

29 December 2023 00:42:53

We assumed that the blister is an elastic body with $\tilde{C}_{ijkl} \approx 0$ and the stress tensor $\sigma_{ij}^{\text{gas}} = P\delta_{ij}$ (where δ_{ij} is the Kronecker delta), which indicates the hydrostatic stress due to the gas pressure P. The relationship between the elastic constant of the matrix C_{ijkl} and $\tilde{C}_{ijkl}$ is shown below, based on Eshelby's equivalent inclusion theory using the Einstein summation convention,[26–28]

$$\sigma_{ij}^{\text{gas}} = C_{ijkl}(S_{klmn}\tilde{e}_{mn} - \tilde{e}_{kl}) = \tilde{C}_{ijkl}(S_{klmn}\tilde{e}_{mn} - \epsilon_{kl}^{\text{gas}}), \quad (1)$$

where S_{klmn} is Eshelby's tensor, $\epsilon_{kl}^{\text{gas}}$ is the corresponding eigenstrain due to the gas pressure, and $\tilde{e}_{mn}$ is the fictitious eigenstrain, which takes the elastic heterogeneity between the blister and matrix material into consideration. Kinoshita et al. reported the general form of Eshelby's tensor for an anisotropic matrix and inclusion as follows:[26,29]

$$S_{klmn} = \frac{1}{8\pi} C_{pqmn} \int_{-1}^{1} d\zeta_3 \int_{0}^{2\pi}$$
$$\times \left(\frac{\xi_l \xi_q N_{kp}(\xi_1, \xi_2, \xi_3) + \xi_k \xi_q N_{lp}(\xi_1, \xi_2, \xi_3)}{D(\xi_1, \xi_2, \xi_3)} \right) d\theta, \quad (2)$$

where

$$D(\xi_1, \xi_2, \xi_3) = P_{pqr}(C_{pj1l}\xi_j\xi_l)(C_{qm2n}\xi_m\xi_n)(C_{rs3t}\xi_s\xi_t),$$

$$N_{km}(\xi_1, \xi_2, \xi_3) = \frac{1}{2} P_{kst} P_{mnr}(C_{sjnl}\xi_l\xi_j)(C_{turv}\xi_u\xi_v),$$

which correspond to the determinant and cofactor of $K_{km} = C_{klmn}\xi_l\xi_n$, respectively, while P_{pqr} denotes the permutation tensor. Using ζ_3 and $\theta, \boldsymbol{\xi} = [\xi_1; \xi_2; \xi_3]$ can be described as follows:

$$\begin{bmatrix} \xi_1 \\ \xi_2 \\ \xi_3 \end{bmatrix} = \begin{bmatrix} \dfrac{\sqrt{1-\zeta_3^2}\,\cos\theta}{a_1} \\ \dfrac{\sqrt{1-\zeta_3^2}\,\sin\theta}{a_2} \\ \dfrac{\zeta_3}{a_3} \end{bmatrix}.$$

The S_{klmn} value can be numerically calculated using Eq. (2). Subsequently, for a given σ_{ij}^{gas}, anisotropic C_{ijkl}, and $\tilde{C}_{ijkl}$ (≈ 0), the simultaneous equation (1) can be solved to derive $\tilde{e}_{kl}$ and $\epsilon_{kl}^{\text{gas}}$ by changing the blister shape (the value of a_i). Using the calculated $\epsilon_{kl}^{\text{gas}}$, the increment in elastic energy ΔE (per unit volume of blister) due to the existence of the blister can be described as follows:

$$\Delta E = -\frac{1}{2} \sigma_{ij}^{\text{gas}} \epsilon_{ij}^{\text{gas}}. \quad (3)$$

By comparing the ΔE values for different blister shapes, we determined the stable blister shape with a minimum of ΔE for the materials with the anisotropic C_{ijkl}. Notably, a small non-zero value must be assigned to $\tilde{C}_{ijkl}$. $\epsilon_{kl}^{\text{gas}}$ cannot be derived using Eq. (1), and ΔE cannot be calculated if $\tilde{C}_{ijkl}$ is simply set at zero. Furthermore, although we investigated the stable shape in terms of elastic energy, some readers may have the concern that the effect of the surface tension (or chemical surface energy) of the materials

on the blister plays a role in determining the blister morphology. Because the size of the observed blisters is usually in the range from a few hundred micrometers to a few millimeters, the dominant energy type involved in this case is the elastic energy, because the elastic energy is volume-dependent and the surface energy is area-dependent. Considering that the surface energy (or surface tension) of conventional materials is of the order of 0.1–1.0 J/m²,[30] the reduction in pressure due to surface tension is lower than the order of MPa and the increase in chemical energy due to the existence of surface ranges from 1.0×10^{-8} to 1.0×10^{-6} J for blisters, which are much smaller than the gas pressure (of the order of GPa) inside the blisters[17] and the order of elastic energy changes (between 1.0×10^{-6} and 1.0×10^{-3} J), which was calculated using our following result.

As mentioned above, the stress field around the blister is critical to understanding the embrittlement of materials, causing cracking. Thus, we calculated the stress field in the matrix material due to the pressure inside the blister using the following equations.[25,31] We numerically calculated the gradient of the displacement $\frac{\partial u_i}{\partial x_j}$ at a certain position $\boldsymbol{x}$ in the matrix due to the blister using the derived $\tilde{e}_{kl}$ as follows:

$$\frac{\partial u_i}{\partial x_j}(\boldsymbol{x}) = C_{klmn}\tilde{e}_{mn} \int_{-1}^{1} d\zeta_3 \int_{0}^{2\pi} \left(\frac{\xi_j \xi_l N_{ik}(\xi_1, \xi_2, \xi_3)}{D(\xi_1, \xi_2, \xi_3)} \right.$$
$$\left. \times \left(\frac{1}{4\pi} U(\boldsymbol{x}\cdot\boldsymbol{\xi}-1) - \frac{1}{2\pi\tilde{x}}\delta(\boldsymbol{x}\cdot\boldsymbol{\xi}-1) \right) \right) d\theta. \quad (4)$$

Here, $U(z)$ is a step function and $\delta(z)$ is a delta function, which are described as follows:

$$U(z) = \begin{cases} 1 & (z \leq 0), \\ 0 & (z > 0), \end{cases}$$

$$\delta(z) = \begin{cases} 1 & (z = 0), \\ 0 & (\text{otherwise}). \end{cases}$$

This limits the range of the integration to $\boldsymbol{x} \cdot \boldsymbol{\xi} \leq 1$ and $\boldsymbol{x} \cdot \boldsymbol{\xi} = 1$ for the first and second terms on the right-hand side, respectively, and $\tilde{x} = \sqrt{(x_1/a_1)^2 + (x_2/a_2)^2 + (x_3/a_3)^2}$. The center of the inclusion is defined at $\boldsymbol{x} = [0, 0, 0]$ in this equation. Based on this equation and

$$\varepsilon_{ij}(\boldsymbol{x}) = \frac{1}{2}\left(\frac{\partial u_i}{\partial x_j} + \frac{\partial u_j}{\partial x_i} \right),$$

the distribution of the total strain can be derived, and eventually, the stress distribution can be derived as $\sigma(\boldsymbol{x}) = C_{ijkl}\varepsilon_{kl}(\boldsymbol{x})$ for the outside of the blister. In general, the position $\boldsymbol{x}$ can be located on both the inside and outside of the blister in the matrix. The above-mentioned equation expresses $\varepsilon_{ij}(\boldsymbol{x}) = S_{ijkl}\epsilon_{kl}^{\text{gas}}$ for the position $\boldsymbol{x}$ inside the ellipsoidal inclusion because $\boldsymbol{x}$ always satisfies $\boldsymbol{x} \cdot \boldsymbol{\xi} < 1$ during integration.

For the detailed setting of the model, $P = -1.0$ GPa was used, thus referring to the order of the pressure inside the hydrogen
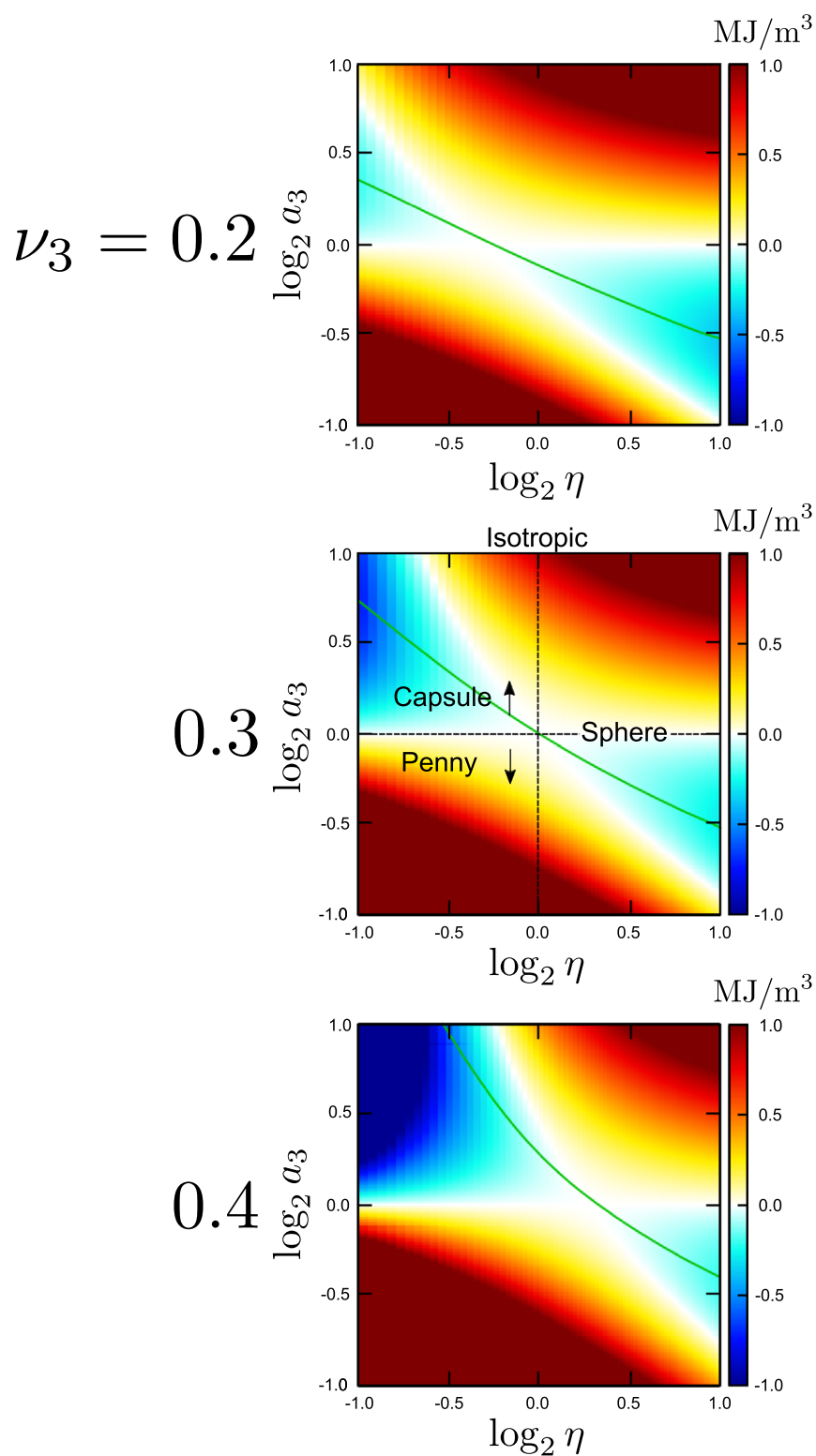
FIG. 1. Elastic energy increment ΔE map with respect to η and a_3 for $\nu_3 = 0.2$, 0.3, and 0.4. Green lines indicate the minimum of ΔE for each η. Note that the zero standard of ΔE is that of the spherical blister for each (η, ν_3).

29 December 2023 00:42:53

blisters in the literature.[17] To simplify the problem, only the anisotropy along the x_3 direction was considered. Thus, the isotropic-form elastic constants, i.e.,

$$C_{ijkl} = \lambda\delta_{ij}\delta_{kl} + \mu(\delta_{ik}\delta_{jl} + \delta_{il}\delta_{jk}),$$

were employed with $\lambda = 60$ GPa and $\mu = 40$ GPa except C_{3333}, C_{1133}, C_{3311}, C_{2233}, and C_{3322}. Thus, we employed

$$C_{3333} = \eta C_{1111}$$

and

$$C_{1133} = C_{3311} = C_{2233} = C_{3322} = \nu_3(C_{1111} + C_{1122}).$$

The anisotropic factor η and ν_3 (Poisson's ratio for x_3 elongation) were varied from 0.5 to 2.0 and from 0.2 to 0.4, respectively. Under these conditions, $\eta = 1.0$ and $\nu_3 = \nu_{iso} = 0.3$ are for the isotropic and cubic materials, respectively, and we can consider hexagonal, tetragonal, and rhombohedral anisotropies, changing these parameters. Notably, Poisson's ratios for the isotropic and cubic materials are also tunable parameters; herein, the ratio is defined as $\nu_{iso} = 0.3$. The effect of ν_{iso} on the shape of the blister is discussed in Appendix B. The anisotropy for shear components is not considered because the pressure inside the blister does not generate the shear stress. The elastic constants of the blister were approximately defined in the following isotropic-form:

$$\tilde{C}_{ijkl} = \frac{1}{1000}[\lambda\delta_{ij}\delta_{kl} + \mu(\delta_{ik}\delta_{jl} + \delta_{il}\delta_{jk})].$$

We confirmed that this condition is robust and performed the same analysis in the following. $\tilde{C}_{ijkl} = \frac{1}{10\,000}[\lambda\delta_{ij}\delta_{kl} + \mu(\delta_{ik}\delta_{jl} + \delta_{il}\delta_{jk})]$ yielded almost the same ΔE map as shown in Fig. 1, and the discussion is the same. Since the anisotropy along the x_3 direction only influences the change in the shape of the blister along the same direction, the values of a_1 and a_2 were fixed at 1.0 and the value of a_3 was varied from 0.5 to 2.0 to model the shape change of the blister. Notably, determining a unit for the half axes is unnecessary because Eshelby's tensor is independent of the inclusion volume. Thus, the positions in this study are unitless. We only calculated the stress field in the first quadrants of x_1–x_2 and x_1–x_3 planes by setting the center of the ellipsoidal inclusion at the origin of the x coordinate system, considering the symmetry of the ellipsoids.

III. RESULTS AND DISCUSSION

Figure 1 presents the calculated ΔE map in terms of the logarithms of η and the half axis of blister a_3 for several ν_3 values, and Fig. 2 presents the shape dependency on elastic anisotropy: the a_3 value with the minimum ΔE (stable shape) at certain η and ν_3 values. Although the spherical shape is optimal for the isotropic elastic constants, as η increased (decreased), the stable blister shifted from a conventional spherical shape to a penny (capsule) shape, e.g., for $(\eta, \nu_3) = (2.0, 0.3)$, the $a_3 = 0.72$ penny is energetically optimal and for $(\eta, \nu_3) = (0.5, 0.3)$, the $a_3 = 1.69$ capsule is optimal. The increase (decrease) in the ν_3 value helped the blister transform a sphere into a capsule (penny). We found that the elastic anisotropy of matrix materials significantly influences the shapes of the blisters, although strong anisotropy is necessary to change the blister
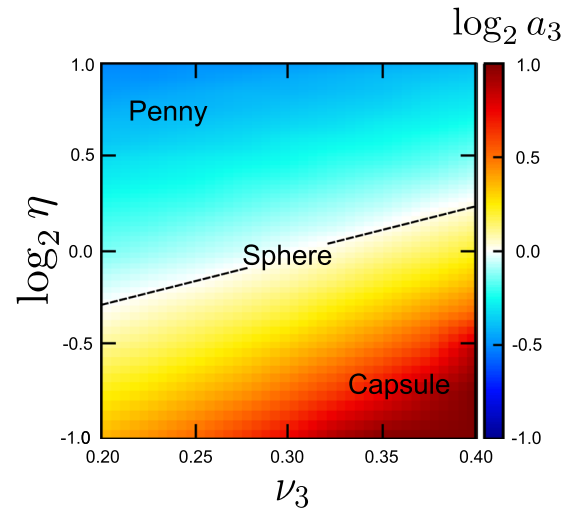

FIG. 2. Change in the a_3 value with the minimum ΔE with respect to η and ν_3.

shape. In particular, a minimum of a 0.1-order change of η or ν_3 is necessary to effect a 0.1-order change of a_3 from the spherical shape. Although this strong anisotropy is not realistic for pure metals, the anisotropic parameter η is expected to have a real value to induce a change in the blister shape for compound or natural materials (such as wood), and this may be realized for the complex alloying metals, such as high-entropy alloys.[32–34] Notably, this study presents only the result with $\nu_{iso} = 0.3$ for the isotropic Poisson's ratio. Moreover, we calculated the ΔE map for $\nu_{iso} = 0.375$ and, in this case, the penny-shaped blister became more favorable than in the $\nu_{iso} = 0.3$ case (the reader can refer to Appendix B for details). In Figs. 3–5, the stress fields calculated for an isotropic sphere $(\eta, \nu_3, a_3) = (1.0, 0.3, 1.0)$, a stable anisotropic penny $(\eta, \nu_3, a_3) = (2.0, 0.3, 0.7)$, and a capsule $(\eta, \nu_3, a_3) = (0.5, 0.3, 1.7)$ are shown, respectively. Although the magnitude of gas pressure was 1.0 GPa, the normal stress field or the hydrostatic stress near the blister in the material was larger than 1.0 GPa; for example, the hydrostatic stress near the spherical blister in the isotropic case was ~1.5 GPa. Moreover, this trend is significant for anisotropic blisters. The value of σ_{33} near the penny-shaped blister and σ_{11}, σ_{22}, and the hydrostatic stress near the capsule-shaped blister were ~3.0 and 2.0 GPa, respectively, which were larger than that for the isotropic sphere. These large stress fields may expand the material and drive new gas atoms inside the blister, which facilitate blister growth and gradual cracking of the material, i.e., embrittlement. These results suggest that the embrittlement due to the blister is more significant for the anisotropic material than for the isotropic or cubic materials. Additionally, for the isotropic sphere, the normal stress fields were anisotropic, although the hydrostatic stress field was isotropic. This trend is similar to the stress field of a Mode I crack as per fracture mechanics[35] and can be attributed to the corresponding normal stress component σ_{ii}^{gas} of the gas pressure. Notably, owing to the possibility that large stress fields are formed around the anisotropic blisters in this study is simply due to the larger C_{3333} of the matrix, we also confirmed that the blister shape has a significant effect (please refer to Appendix A).
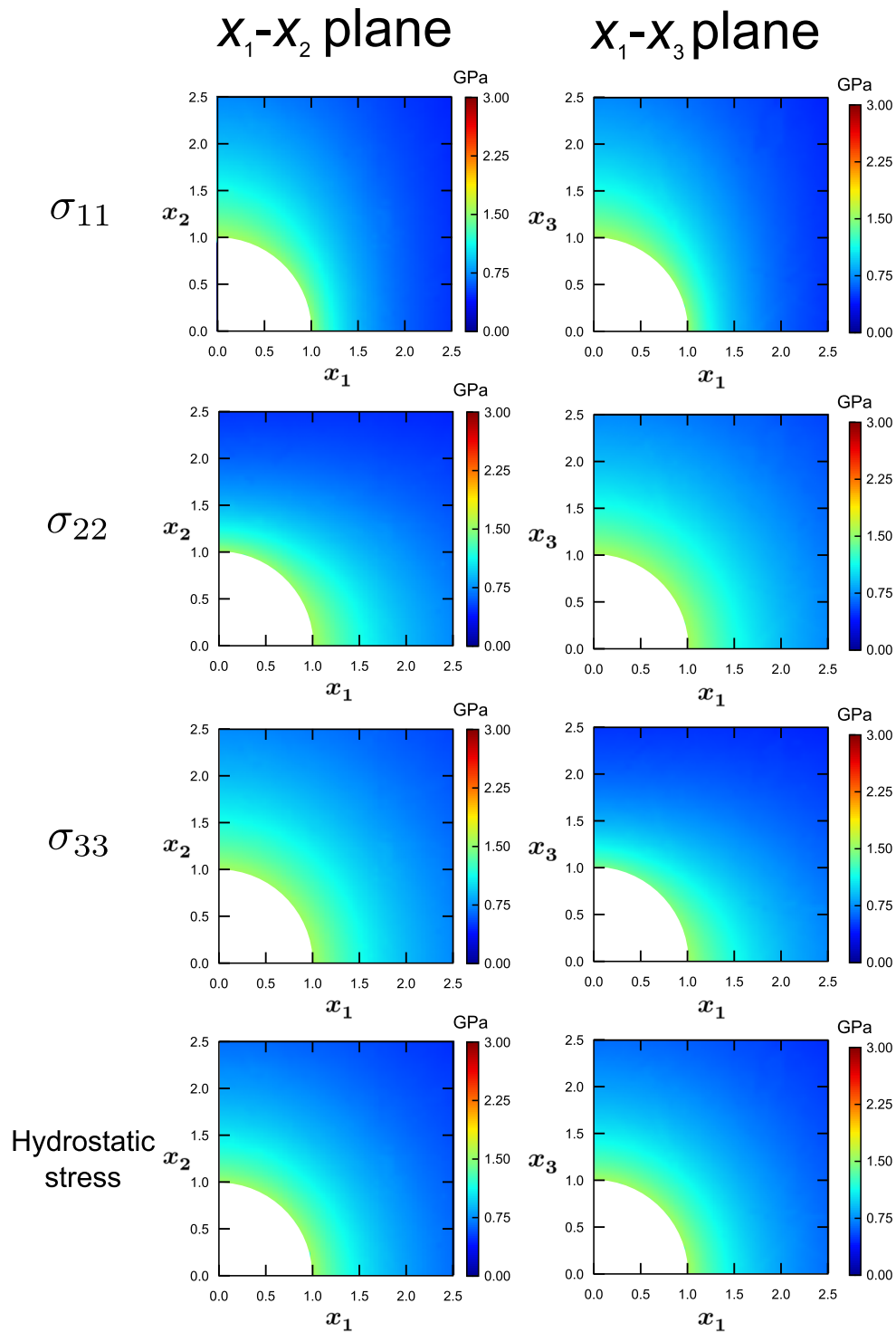
Sphere

FIG. 3. Normal stress fields around the spherical blister using isotropic elastic constants: $(\eta, \nu_3, a_3) = (1.0, 0.3, 1.0)$.

29 December 2023 00:42:53

Penny

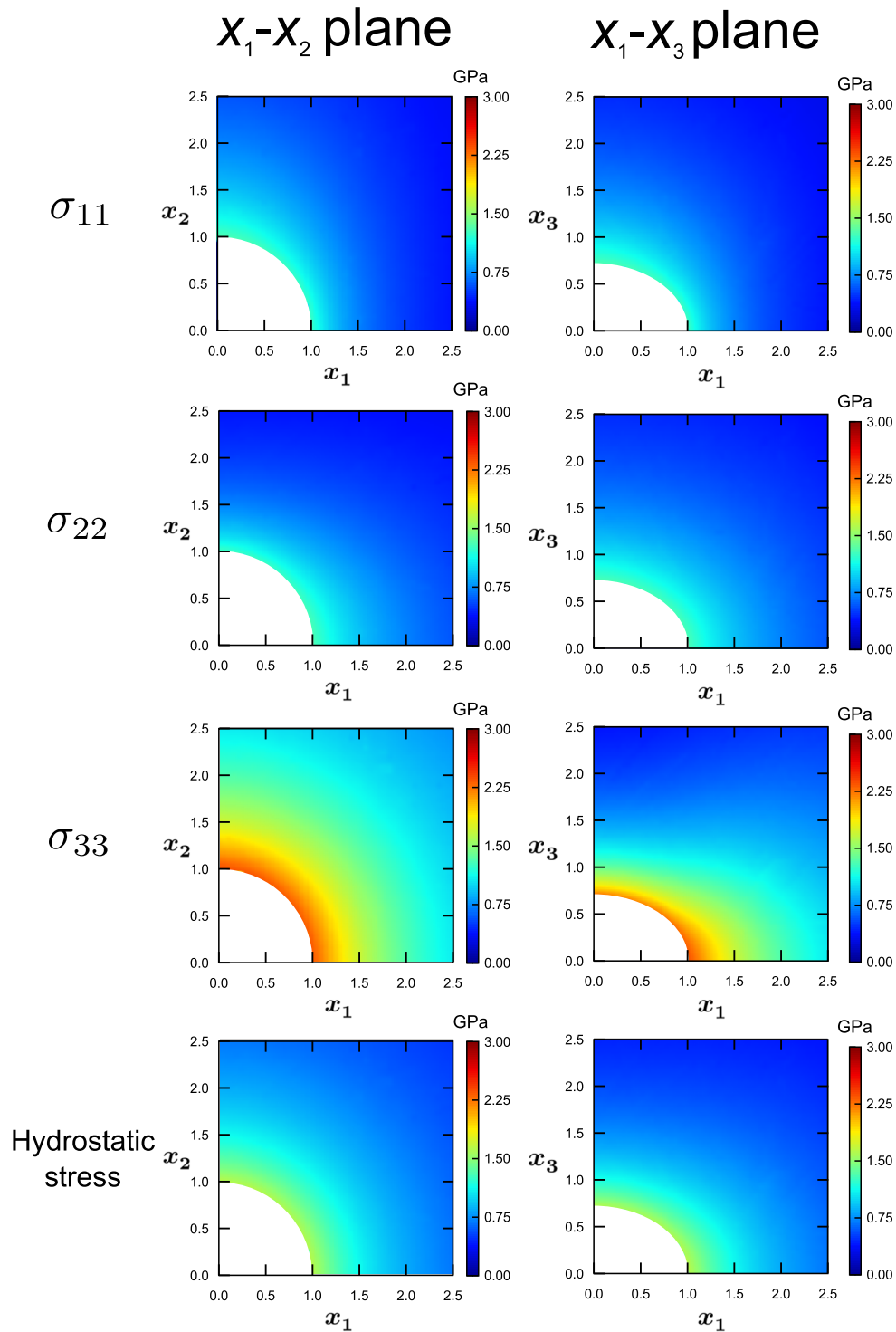## x_1-x_2 plane x_1-x_3 plane

FIG. 4. Normal stress fields around the stable penny-shaped blister using anisotropic elastic constants: $(\eta, \nu_3, a_3) = (2.0, 0.3, 0.7)$.
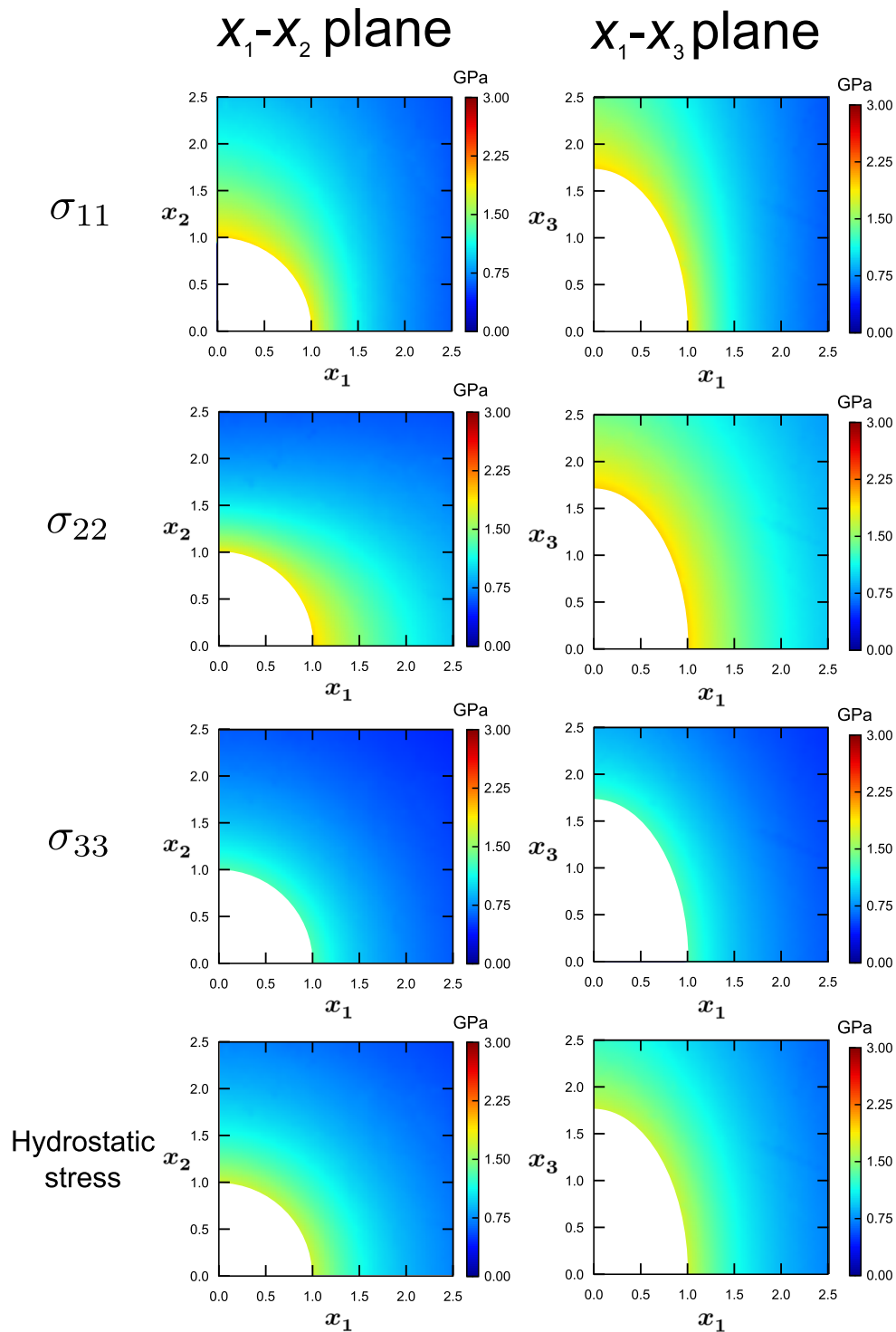
Capsule

FIG. 5. Normal stress fields around the stable capsule-shaped blister using anisotropic elastic constants: $(\eta, \nu_3, a_3) = (0.5, 0.3, 1.7)$.
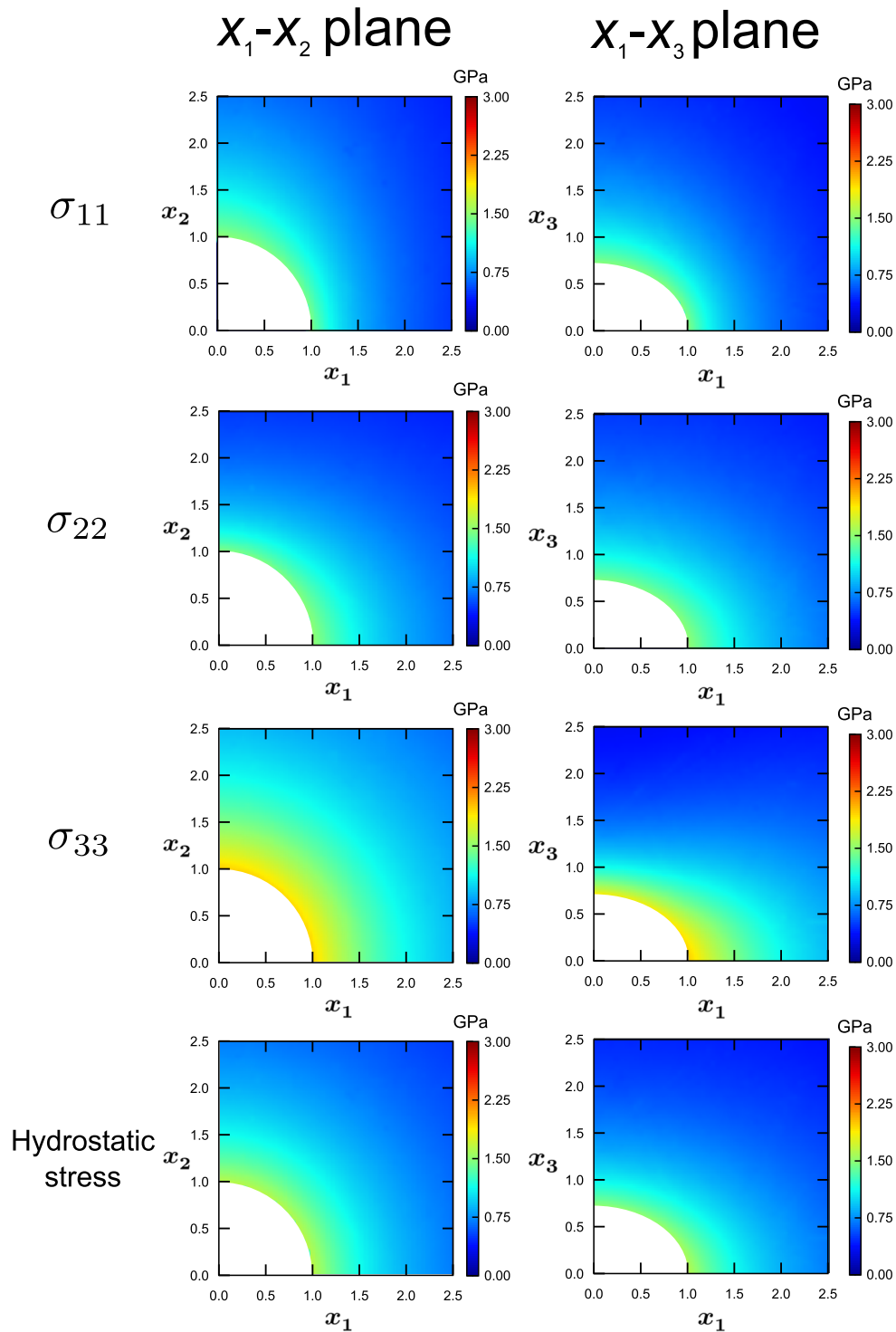
29 December 2023 00:42:53

Penny

FIG. 6. Stress fields around the penny-shaped blister using isotropic elastic constants: $(\eta, \nu_3, a_3) = (1.0, 0.3, 0.7)$.
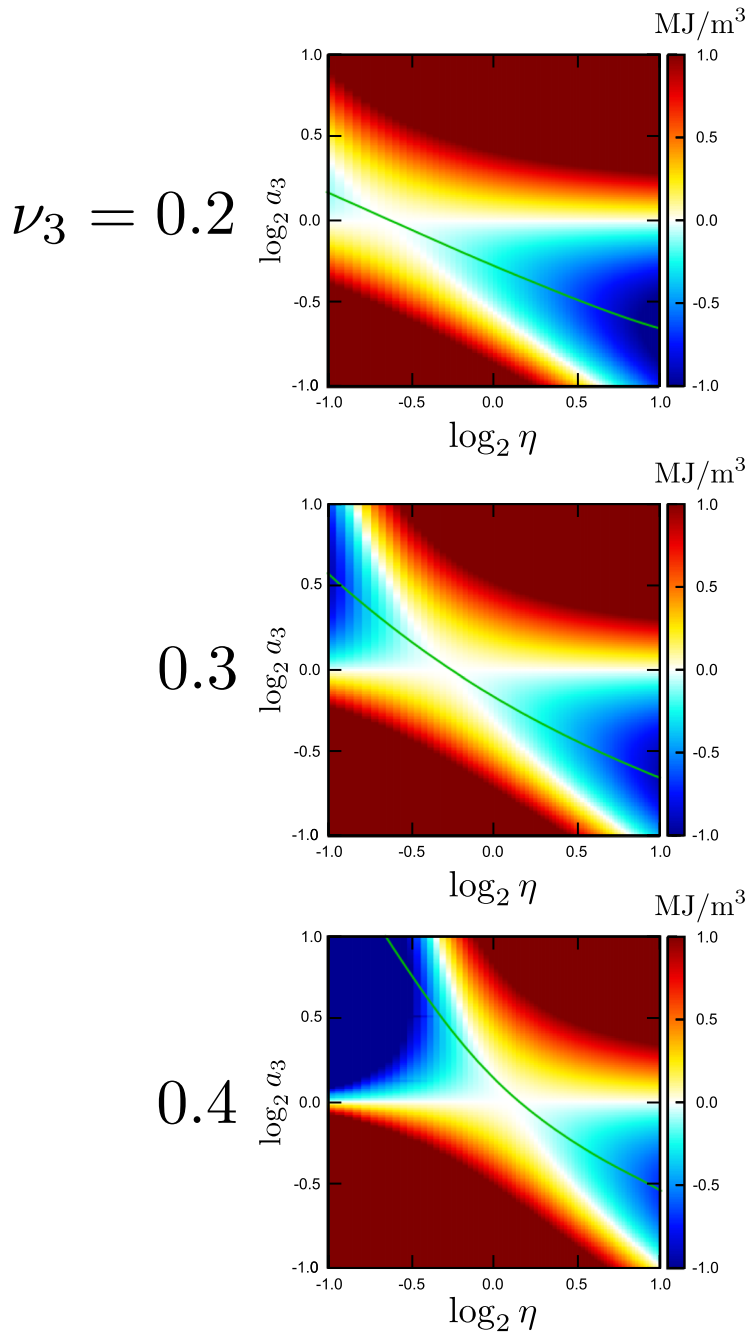
29 December 2023 00:42:53

FIG. 7. Elastic energy increment ΔE map in terms of η and a_3 for $\nu_3 = 0.2, 0.3$, and 0.4 using $\mu = 20$ GPa, which corresponds to a Poisson's ratio of the isotropic elastic constants $\nu_{iso} = 0.375$. Green lines indicate the minimum of ΔE for each η. The zero standard of ΔE is that of the spherical blister for each (η, ν_3).

IV. CONCLUSION

In summary, the stable shapes of constant-pressure blisters in anisotropic materials (hexagonal, tetragonal, and rhombohedral) were investigated in terms of energy based on continuum theory (micromechanics), considering the blister as Eshelby's ellipsoidal inclusion. The non-negligible change in the blister shape was confirmed in terms of the anisotropic factor $\eta \equiv C_{3333}/C_{1111}$. Although the spherical shape is optimal for isotropic and cubic materials ($\eta = 1$), the x_3 normal penny and capsule shapes are theoretically confirmed to be stable for $\eta > 1$ and $\eta < 1$, respectively. We confirmed that the penny- and capsule-shaped blisters generated larger stress fields around themselves than the sphere blisters, causing cracks. Thus, the embrittlement due to the encapsulated gas (generally, hydrogen or helium) for the anisotropic materials would be

more significant than the isotropic and cubic ones. Although we did not investigate the shapes in the orthorhombic, monoclinic, and triclinic cases, the anisotropy of C_{2222} can be assumed to influence a_2 and generate a more complex ellipsoidal blister ($a_1 \neq a_2 \neq a_3$).

ACKNOWLEDGMENTS

AUTHOR DECLARATIONS

Conflict of Interest

The author has no conflicts to disclose.

Author Contributions

Akio Ishii: Conceptualization (equal); Formal analysis (equal); Funding acquisition (equal); Investigation (equal); Methodology (equal); Software (equal); Validation (equal); Visualization (equal); Writing – original draft (equal); Writing – review & editing (equal).

DATA AVAILABILITY

The data supporting the findings of this study are available from the corresponding author upon reasonable request.

APPENDIX A: STRESS FIELD AROUND THE PENNY BLISTER IN ISOTROPIC MATERIALS

Although we found that the large stress field in the anisotropic case is due to the shape of the blister, large stress fields around the anisotropic blister may be simply due to the larger C_{3333} of the matrix because C_{3333} value increases with increasing anisotropy under the conditions of our calculations. To confirm this, we calculated the stress field of the penny-shaped blister using isotropic elastic constants $(\eta, \nu_3, a_3) = (1.0, 0.3, 0.7)$, and the result is shown in Fig. 6. Although the stress field was lower than that of the penny-shaped blister using anisotropic elastic constants as shown in Fig. 4 (*vide supra*), the stress field was larger than that of the spherical blister shown in Fig. 3. Thus, we concluded that the blister shape significantly influences the stress field around it.

APPENDIX B: EFFECT OF POISSON'S RATIO OF ISOTROPIC ELASTIC CONSTANTS (ν_{iso})

In the main text, we only presented the result with $\nu_{\text{iso}} = 0.3$ for isotropic Poisson's ratio, and we did not discuss the effect of ν_{iso} on the shape of the blister. To investigate this effect, we calculated the ΔE map for $\mu = 20$ GPa, which corresponds to the isotropic Poisson's ratio $\nu_{\text{iso}} = 0.375$ and increased from 0.3, as shown in Fig. 7. Compared with Fig. 1 in the main text, the penny (capsule)-shaped blister was more (less) optimal. The opposite effect would be observed if we decreased ν_{iso} from 0.3.

REFERENCES

[1] W. D. Wilson, C. L. Bisson, and M. I. Baskes, "Self-trapping of helium in metals," Phys. Rev. B **24**, 5616–5624 (1981).

[2] B. Singh and H. Trinkaus, "An analysis of the bubble formation behaviour under different experimental conditions," J. Nucl. Mater. **186**, 153–165 (1992).

[3] J. B. Condon and T. Schober, "Hydrogen bubbles in metals," J. Nucl. Mater. **207**, 1–24 (1993).

[4] H. Trinkaus and B. N. Singh, "Helium accumulation in metals during irradiation—Where do we stand?," J. Nucl. Mater. **323**, 229–242 (2003).

[5] J. Chen, J. Wang, E. Han, J. Dong, and W. Ke, "States and transport of hydrogen in the corrosion process of an AZ91 magnesium alloy in aqueous solution," Corros. Sci. **50**, 1292–1305 (2008).

[6] H. Toda, T. Hidaka, M. Kobayashi, K. Uesugi, A. Takeuchi, and K. Horikawa, "Growth behavior of hydrogen micropores in aluminum alloys during high-temperature exposure," Acta Mater. **57**, 2277–2290 (2009).

[7] W. Geng, L. Wan, J.-P. Du, A. Ishii, N. Ishikawa, H. Kimizuka, and S. Ogata, "Hydrogen bubble nucleation in α-iron," Scr. Mater. **134**, 105–109 (2017).

[8] J. Hou, X. S. Kong, J. Sun, Y. W. You, X. Wu, C. S. Liu, and J. Song, "Hydrogen bubble nucleation by self-clustering: Density functional theory and statistical model studies using tungsten as a model system," Nucl. Fusion **58**, 096021 (2018).

[9] J. Hou, X.-S. Kong, X. Wu, J. Song, and C. S. Liu, "Predictive model of hydrogen trapping and bubbling in nanovoids in bcc metals," Nat. Mater. **18**, 833–839 (2019).

[10] L. Wan, W. T. Geng, A. Ishii, J.-P. Du, Q. Mei, N. Ishikawa, H. Kimizuka, and S. Ogata, "Hydrogen embrittlement controlled by reaction of dislocation with grain boundary in alpha-iron," Int. J. Plast. **112**, 206–219 (2019).

[11] J. Hou, X. S. Kong, C. S. Liu, and J. Song, "Hydrogen clustering in bcc metals: Atomic origin and strong stress anisotropy," Acta Mater. **201**, 23–35 (2020).

[12] J. M. Polfus, O. M. Løvvik, R. Bredesen, and T. Peters, "Hydrogen induced vacancy clustering and void formation mechanisms at grain boundaries in palladium," Acta Mater. **195**, 708–719 (2020).

[13] J.-P. Du, W. T. Geng, K. Arakawa, J. Li, and S. Ogata, "Hydrogen-enhanced vacancy diffusion in metals," J. Phys. Chem. Lett. **11**, 7015–7020 (2020).

[14] K. Arakawa, A. Kageyama, H. Hiroshima, H. Yasuda, and S. Ogata, "Hydrogen effects on the migration of nanoscale cavities in iron," ISIJ Int. **61**, 2305–2307 (2021).

[15] C. E. Zapffe and C. A. Sims, "Internal stress and defects in steel," Trans. AIME **145**, 225–261 (1941).

[16] A. Griesche, E. Dabah, T. Kannengiesser, N. Kardjilov, A. Hilger, and I. Manke, "Three-dimensional imaging of hydrogen blister in iron with neutron tomography," Acta Mater. **78**, 14–22 (2014).

[17] M. C. Tiegel, M. L. Martin, A. K. Lehmberg, M. Deutges, C. Borchers, and R. Kirchheim, "Crack and blister initiation and growth in purified iron due to hydrogen loading," Acta Mater. **115**, 24–34 (2016).

[18] X. Tao, G. C. Lv, J. Kou, X. Xiong, A. A. Volinsky, C. S. Ku, K. Chen, and Y. J. Su, "Synchrotron X-ray Laue diffraction study of hydrogen-induced blisters on iron grain boundaries," Scr. Mater. **169**, 82–86 (2019).

[19] W. Q. Chen, X. Y. Wang, K. L. Li, Y. N. Wang, T. W. Morgan, B. Xu, Y. L. Chiu, and W. Liu, "Nucleation mechanism of intra-granular blisters in tungsten exposed to hydrogen plasma," Scr. Mater. **187**, 243–249 (2020).

[20] Y. Ueda, T. Funabiki, T. Shimada, K. Fukumoto, H. Kurishita, and M. Nishikawa, "Hydrogen blister formation and cracking behavior for various tungsten materials," J. Nucl. Mater. **337–339**, 1010–1014 (2005).

[21] X. G. Hu, Q. Zhu, S. P. Midson, H. V. Atkinson, H. B. Dong, F. Zhang, and Y. L. Kang, "Blistering in semi-solid die casting of aluminium alloys and its avoidance," Acta Mater. **124**, 446–455 (2017).

[22] A. Ishii, "*Ab initio* morphology prediction of Zr hydride precipitates using atomistically informed Eshelby's ellipsoidal inclusion," Comput. Mater. Sci. **211**, 111500 (2022).

[23] A. Ishii, "Elastic investigation for the existence of B33 phase in TiNi shape memory alloys using atomistically informed Eshelby's ellipsoidal inclusion," Comput. Mater. Sci. **218**, 111954 (2023).

[24] A. Ishii, "*Ab initio* prediction of temperature-dependent stability of heterogeneous B19′ phase in TiNi alloy using atomistically informed Eshelby's ellipsoidal inclusion," Mater. Today Commun. **35**, 105861 (2023).

[25] A. Ishii, "Morphology prediction of elastically interacting Zr hydride precipitates and cracks in α-Zr using atomistically informed Eshelby's ellipsoidal inclusion," Comput. Mater. Sci. **231**, 112568 (2024).

[26] T. Mura, *Micromechanics of Defects in Solids* (Springer Science & Business Media, 2013).

[27] J. D. Eshelby, "The determination of the elastic field of an ellipsoidal inclusion, and related problems," Proc. R. Soc. London, Ser. A **241**, 376–396 (1957).

[28] J. D. Eshelby, "Elastic inclusions and inhomogeneities," in *Progress Solid Mechanics*, edited by I. N. Sneddon and R. Hill (North-Holland, Amsterdam, 1961), Vol. 2, pp. 89–140.

[29] N. Kinoshita and T. Mura, "Elastic fields of inclusions in anisotropic media," Phys. Status Solidi A **5**, 759–768 (1971).

[30] A. Jain, S. P. Ong, G. Hautier, W. Chen, W. D. Richards, S. Dacek, S. Cholia, D. Gunter, D. Skinner, G. Ceder, and K. A. Persson, "Commentary: The Materials Project: A materials genome approach to accelerating materials innovation," APL Mater. **1**, 011002 (2013).

[31] T. Mura and P. C. Cheng, "The elastic field outside an ellipsoidal inclusion," J. Appl. Mech. **44**, 591–594 (1977).

[32] Y. Wu, W. H. Liu, X. L. Wang, D. Ma, A. D. Stoica, T. G. Nieh, Z. B. He, and Z. P. Lu, "*In-situ* neutron diffraction study of deformation behavior of a multi-component high-entropy alloy," Appl. Phys. Lett. **104**, 051910 (2014).

[33] T. Teramoto, K. Yamada, R. Ito, and K. Tanaka, "Monocrystalline elastic constants and their temperature dependences for equi-atomic Cr-Mn-Fe-Co-Ni high-entropy alloy with the face-centered cubic structure," J. Alloys Compd. **777**, 1313–1318 (2019).

[34] C.-C. Yen, G.-R. Huang, Y.-C. Tan, H.-W. Yeh, D.-J. Luo, K.-T. Hsieh, E.-W. Huang, J.-W. Yeh, S.-J. Lin, C.-C. Wang, C.-L. Kuo, S.-Y. Chang, and Y.-C. Lo, "Lattice distortion effect on elastic anisotropy of high entropy alloys," J. Alloys Compd. **818**, 152876 (2020).

[35] G. Chell, *Developments in Fracture Mechanics* (Applied Science Publishers, 1979), Vol. 1.

29 December 2023 00:42:53